Deep-going reconstruction of Ir(100)-5 × 1

2002 J. Phys.: Condens. Matter 14 12353

(http://iopscience.iop.org/0953-8984/14/47/310)

INSTITUTE OF PHYSICS PUBLISHING JOURNAL OF PHYSICS: CONDENSED MATTER

J. Phys.: Condens. Matter **14** (2002) 12353–12365 PII: S0953-8984(02)53966-7

Deep-going reconstruction of Ir(100)-5 × 1

A Schmidt, W Meier, L Hammer and K Heinz

Lehrstuhl für Festkörperphysik, Universität Erlangen-Nürnberg, Staudtstr. 7, D-91058 Erlangen, Germany

E-mail: kheinz@fkp.physik.uni-erlangen.de

Received 26 September 2002
Published 15 November 2002
Online at stacks.iop.org/JPhysCM/14/12353

Abstract

We present a new investigation of the metastable 1 × 1 and reconstructed 5 × 1 phases of Ir(100) using quantitative low-energy electron diffraction and scanning tunnelling microscopy. It is shown that the 5 × 1 reconstruction of Ir(100) extends up to the fourth layer into the surface. This structural information is retrieved by the use of electron energies up to 600 eV which simultaneously provides an unusually broad database of more than 10.000 eV. Together with an excellent quality of the theory–experiment fit equivalent to an R-factor of $R_P = 0.144$ this allows for rather small error limits of the as many as 17 structural parameters describing the four-layer reconstructed surface. Similar features hold for the 1 × 1 phase which is analysed in parallel. In addition, we present a systematic investigation of the influence of the electron energy range applied and of the allowed depth of reconstruction on the accuracy of the analysis. It appears that for the case of Ir(100)-5 × 1 the structural parameters describing the top two layers are largely independent from the consideration of the reconstruction of deeper layers.

(Some figures in this article are in colour only in the electronic version)

1. Ir(100)-5 × 1—a well known surface reconstruction to be revisited

The surface reconstruction type of Ir(100) has been known for a long time [1]: top-layer atoms are rearranged off their quadratic bulklike positions to form a hexagonal overlayer. This has been confirmed both by quantitative low-energy electron diffraction (LEED) [2–6] and first-principles calculations using density functional theory (DFT) [7]. Additionally, in these papers the overlayer's registry with respect to the substrate was identified as indicated in figure 1 ('two-bridge model') and this layer's buckling induced by the incoherence with the substrate was quantitatively determined. The buckled two-bridge model has also been confirmed by investigations using the scanning tunnelling microscope (STM) [8]. More recently, it has been shown by Johnson *et al* again applying quantitative LEED [6] that the reconstruction is not confined to the top layer, but extends to the second layer which is also

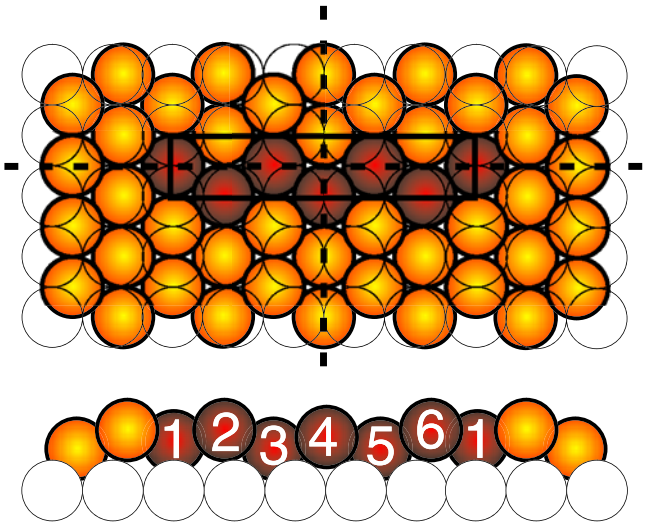

Figure 1. Reconstruction model of Ir(100)-5 × 1 in top and side views with the unit mesh indicated by the solid-line rectangle and dark-shaded atoms. The name 'two-bridge model' stems from the fact that within the unit cell two atoms of the hexagonal overlayer (nos 1 and 4) reside exactly in bridge positions of the substrate. The applicable mirror planes are indicated by broken lines.

buckled. Allowing additionally for some lateral atomic relaxations in the top layer made the quality of the theory–experiment fit improve substantially. Whilst the overall buckling amplitude of the top layer was determined to be about 0.5 Å [2–6], the buckling resulting for the second layer is 0.09 Å only [6]. At a first glance this fast decrease suggests that buckling amplitudes of deeper layers should be negligible, if not completely vanishing.

It was therefore to our surprise that—in connection with the characterization of the clean surface before carrying out epitaxial growth experiments—we could not fit the measured LEED intensities with the above two-layer reconstruction model of [6] when increasing the electron energy up to 600 eV. On the other hand, the fit was of the same quality as in [6] when we used data of the same maximum energy, i.e. 300 eV. This indicates that, unexpectedly, also deeper layers must be reconstructed. Seemingly, they are probed with sufficient weight only at higher energies, i.e., for higher electron penetration.

We therefore undertook a completely new LEED analysis in order to retrieve the full reconstruction of Ir(100)-5 × 1 by using data up to 600 eV. This is equivalent to an accumulated database width of more than 10.000 eV which, to our knowledge, is unparalleled up to now. Additionally, such an investigation is also of methodical importance, in particular as it promises to illuminate the issue of parameter correlations in the sense of whether or not the structural parameters obtained for the top two layers can be retrieved accurately independent of the depth of reconstruction considered in the analysis. Moreover, we extended the investigations to the 1 × 1 structure of Ir(100) which can be prepared as a metastable phase [9–11] and which—with all layers unreconstructed—should be unsuspicious: the same interlayer spacings d_{ik} should result as for lower energies, in particular as d_{34} has been found to be already almost bulklike [6].

For both the 1 × 1 and 5 × 1 phases the LEED work was accompanied by investigations using the STM with atomic resolution. It informs us about the surface morphology and crystallographic quality of the surfaces as well as about the accommodation of the extra atoms of the hexagonal top layer when the reconstruction is lifted to form the 1 × 1 phase.

2. Experimental and computational details

The experiments were performed using a stainless steel ultrahigh-vacuum vessel equipped with an STM (beetle type, RHK) and a back-view three-grid LEED optics with easy sample exchange between the two stages. The sample surface was sputtered by 2 keV Ar^+ ions followed by annealing at 1300 K in an O_2-atmosphere of 2×10^{-7} mbar. This produced sharp and low-background 5×1 diffraction patterns with equally weighted orthogonal domains and no impurities detectable by Auger electron spectroscopy (AES). Due to the very good orientation of the surface (better than 0.1°), very large and flat domains with widths of several thousand Ångstroms appeared in the STM. The metastable 1×1 phase was prepared as described earlier [11], i.e. by annealing the reconstructed surface in 5×10^{-7} mbar O_2 at 470 K for 2 min followed by a flash to 750 K and subsequent heating in 5×10^{-7} mbar H_2 at 530 K for 1 min.

LEED intensity data were taken at normal incidence of the primary beam and the sample at about 100 K using a CCD video camera operated under computer control. Full diffraction images were stored on hard disk in steps of 0.5 eV between 20 and 600 eV allowing for total measuring times of about 15 min independent of the complexity of the patterns. The intensity spectra of individual beams resulted by off-line evaluation whereby symmetrically equivalent beams were averaged as usual. The energy width of all accumulated inequivalent beams amounts to $\Delta E = 2.317$ eV for the 1×1 phase and to $\Delta E = 10.508$ eV for the 5×1 phase.

The model intensity calculations to fit the experimental diffraction data were carried out using the perturbation method tensor LEED [12–14]. The program package TensErLEED [15] was applied, which allows for the easy variation of both geometrical and vibrational parameters. Relativistically calculated and spin-averaged phase shifts were used up to $l_{max} = 13$ for energies up to 600 eV. Electron attenuation was simulated by an imaginary part of the inner potential which, adjusted for the best fit, turned out to be $V_{0i} = 5.0$ eV. The real part of the inner potential, V_{0r}, was allowed to vary with energy because of the large energy range covered and in view of the energy dependence of the exchange correlation potential. Following a formula given by Rundgren [16], the dependence $V_{0r} = V_{00}+\max[-11.48, 0.12-83.64(E/eV+2.94)^{1/2}]$ eV was applied with the value of V_{00} varied during the course of the theory–experiment fit. The program package [15] also contains an automated structural search based on a frustrated simulated annealing procedure [17] guided by the Pendry R-factor [18]. The latter's variance, $\mathrm{var}(R_P)$, was used to estimate error limits for the parameters determined.

3. The metastable 1 × 1 phase

3.1. Appearance in the STM

In the equilibrated 5×1 phase, the atomic density in the hexagonal top layer is 20% higher than in an unreconstructed quadratic bulk layer (see figure 1). When the surface reconstruction is lifted to form the metastable 1×1 phase as described above, the corresponding extra atoms must be accommodated at steps or in islands. We observed both cases as demonstrated in figure 2.

On the one hand, rectangular and often nearly quadratic islands can develop on large scale terraces (figure 2(a)). From the evaluation of line profiles the island height turns out to be 1.87 Å, within the error limits of STM calibration agreeing with the Ir(100) interlayer spacing (1.92 Å). Additionally, however, there are very long straight and rather thin lines parallel to the step edges as better visible in the zoomed-in image given in figure 2(b). Both the islands and

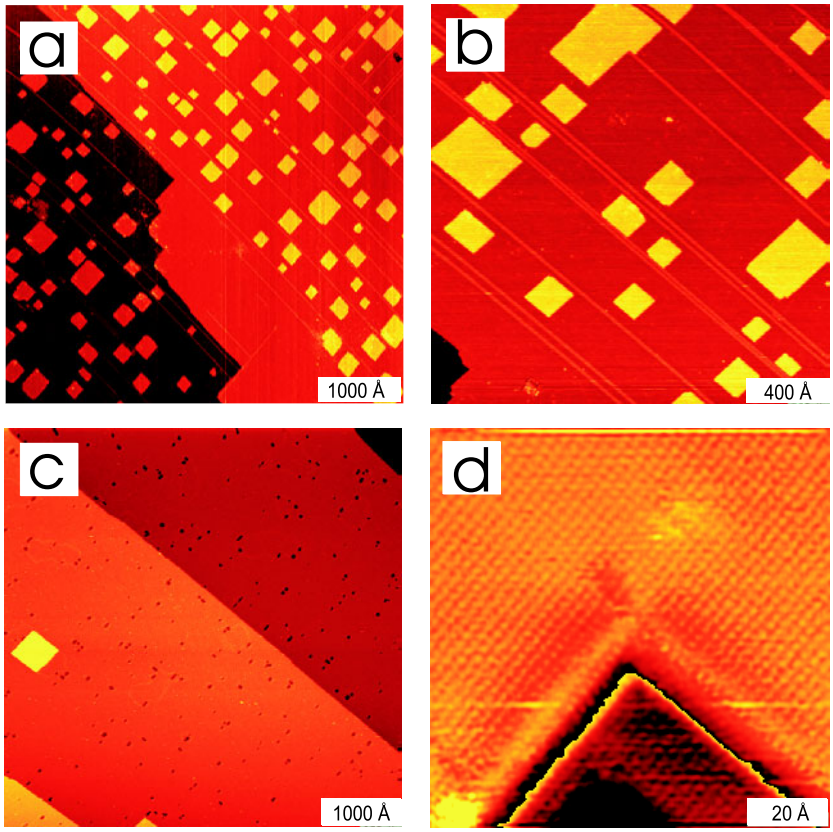

Figure 2. STM images of the 1 × 1 phase as prepared according to the recipe described in the text. Slight (uncontrolled) variations of preparation conditions cause different states with adatom islands (a), (b) or vacancy agglomerations (c) dominating. The latter can extend even to the second layer ((d), contrast amplified).

lines were observed earlier [8]. The islands are always arranged between the lines, i.e., they are never grown over them. Obviously, within the surface deconstruction process and at the limited temperatures applied ($\leqslant$750 K) these lines act as diffusion barriers. The line height as appearing in the STM amounts to about 0.5 Å, which is close to the buckling amplitude of the reconstructed top layer [5, 6]. So, the lines might be residua of the former surface reconstruction or nucleation centres of a renewed reconstruction process towards 5 × 1 induced by a slightly too high annealing temperature in the preparation process of the 1 × 1 phase. In fact, earlier LEED measurements [11] of the transition 1 × 1 → 5 × 1 could be interpreted by shifts of atomic rows along the row direction, leading to such surface protruding lines as indicated in figure 3(a). They were observed even with atomic resolution in STM investigations [19] of the (100) surface of a NiPt alloy which undergoes basically the same reconstruction as Pt(100). The latter reconstruction is very similar to that of Ir(100) [20], in particular the initial reconstruction process starting from the 1 × 1 phase appears to be the same [21].

The role of the lines as diffusion barriers is consistent with the observation that large areas adjacent to step edges are free of islands when they contain no such lines. This is apparent from the middle part of figure 2(a). In this area, the extra atoms released from the reconstruction layer can diffuse to the step edge (even when as distant as 10^3 Å) *and* can cross the edge, i.e. there is

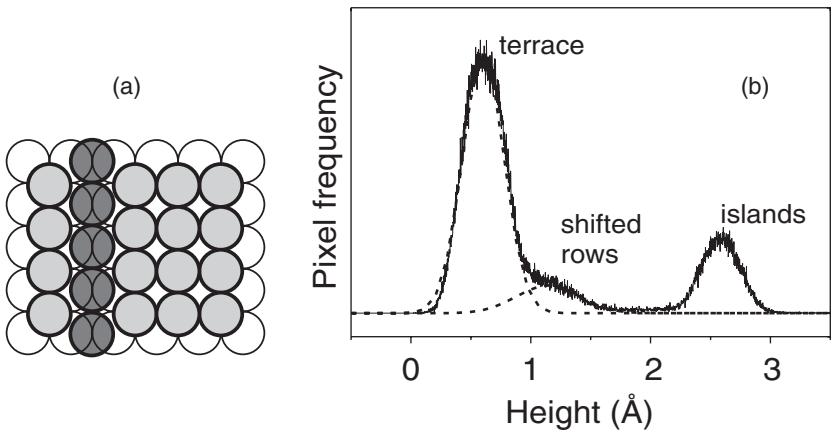

Figure 3. (a) Model of the initial state of the reconstruction process with a single atomic row of the 1 × 1 phase shifted. (b) Evaluation of the pixel height from images such as figure 2(a).

no Ehrlich–Schoebel barrier effective, in contrast to the findings on many other surfaces (see e.g. [22]). For the ratio r between island and terrace areas the evaluation of images like that in figure 2(a) using a pixel height distribution (figure 3(b)) yields $r = 18.0 \pm 0.7\%$. This is only slightly below the maximum value of 20% which indicates that only a small fraction of the extra atoms have diffused to steps.

Occasionally, the preparation of the 1 × 1 phase led to surfaces with almost island free unreconstructed terraces as displayed in figure 2(c). This is even though the same overall preparation recipe was applied to produce the 1 × 1 phase, so the modified state observed is due to only small (uncontrolled) variations of the preparation conditions. Obviously, the large majority of extra atoms released from the reconstructed layer has diffused to step edges. Yet, in the case displayed in figure 2(c) there are also agglomerations of vacancies which, as magnified in panel (d), can even extend to the second layer. Their appearance might be a consequence of the chemical treatment of the surface in order to initiate the deconstruction process, but with more detailed information lacking this remains a speculation. Independent of the kind of 1 × 1 phase prepared, however, there are always well ordered 1 × 1 domains with sizes considerably larger than the coherence length of LEED electrons (typically 100 Å), so that these surfaces are well suited for a crystallographic LEED analysis.

3.2. Structure analysis

For the intensity analysis the first four interlayer spacings $d_{i,i+1} (i = 1, \ldots, 4)$ were varied whilst deeper spacings were fixed at the bulk value, $d_b = 1.92$ Å. As non-structural parameters the (isotropic) vibrational amplitude of top-layer atoms, v_1, and the amplitude common to all atoms below, v_b, were included in the fit. The structural search converged very quickly resulting in a best-fit Pendry R-factor of $R_P = 0.115$. This is about the same quality of fit as obtained earlier [6], except that the present database extends to much higher energies (600 versus 300 eV) with the increased risk to miss spectral features. The low R-factor is consistent with an evenly favourable optical comparison over the full energy range as demonstrated for two selected beams in figure 4. Evidently, the data fit in the low-(<300 eV) and high-(>300 eV) energy ranges is of the same quality.

The resulting best-fit structural and vibrational parameters are comprised in table 1 together with the error limits as estimated from the variance of the R-factor (var$(R_P) = 0.015$),

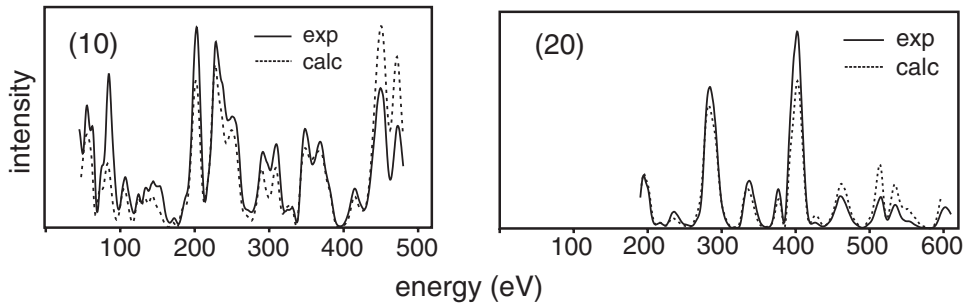

Figure 4. Comparison of experimental and calculated best-fit spectra for the metastable 1×1 phase of Ir(100) for two selected beams.

Table 1. LEED results for the first few interlayer spacings $d_{i,k}$ (together with the percentage change relative to the bulk value $d_b = 1.92$ Å) and the vibrational amplitudes in the top surface layer (v_s) and the layers below (v_b) in the 1×1 phase of Ir100).

	d_{12} (Å)	d_{23} (Å)	d_{34} (Å)	d_{45} (Å)	v_1 (Å)	v_b (Å)
This work	1.85 ± 0.01	1.94 ± 0.01	1.92 ± 0.01	1.93 ± 0.01	0.060 ± 0.02	0.045 ± 0.03
	-3.6%	$+1.0\%$	$\pm 0.0\%$	$+0.5\%$		
[6]	1.83 ± 0.03	1.94 ± 0.03	1.91 ± 0.03	1.92(fixed)		
	-4.5%	$+1.3\%$	-0.3%			

neglecting, however, correlations between parameters (as usual). Also, comparison is made with recent results given in [6]. As usual for fcc(100) surfaces there is an oscillatory and quickly decaying multilayer relaxation with the first spacing contracted. The vibrational amplitude of bulk atoms, v_b, determined for the sample temperature at measurement ($\approx$100 K) corresponds quantitatively to the bulk Debye temperature of Ir (420 K). The increased value for the top layer, v_s, is in line with the frequently observed enhancement by $\sqrt{2}$. Our structural results agree with those of [6] within the limits of errors given. Yet, our error limits are substantially lower though the minimum R-factor is about the same (0.115 versus 0.126 [6]). There are two reasons for this: first, the database ΔE we use is considerably broader (2.317 versus 860 eV [6]). Second, due to higher energies (smaller wavelengths) used, the R-factor curve is steeper, i.e., there is a higher structural sensitivity.

4. The reconstructed 5×1 phase

4.1. Appearance in the STM

The reconstruction of Ir(100)-5×1 is clearly visible in the STM. At comparably low resolution (figure 5, left), there are equidistant bright lines separated by dark ones. Correspondence of these lines can be made to the two-bridge-site model (figure 1) repeated below the STM image with the proper atomic shading: a bright line is caused by the two atomic rows with atoms in almost top positions with the bridge-site row between them unresolved. A dark line corresponds to rows with atoms in near-hollow positions, again with the bridge-site row in between unresolved. With better resolution (figure 5, right), the bridge-site row within the dark line is resolved and the bright line splits up in images of the two top-site rows with, however, the bridge-site row between them remaining unresolved.

The close correspondence between the STM images and the surface buckling according to the two-bridge-site model confirms this model as also found earlier by STM [8]. Yet, as argued

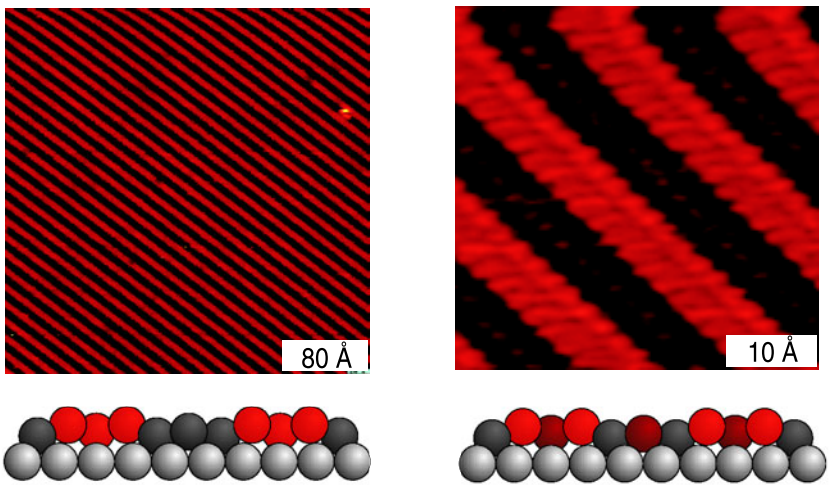

Figure 5. STM images of the 1 × 1 reconstruction taken at low (left) and higher (right) resolution. Atoms representing the appearing atomic rows are given by different shadings corresponding to the model displayed in figure 1.

in the introductory paragraph, important features of the reconstruction are still missing (even with a second-layer reconstruction included [6]), demanding a more complete crystallographic analysis.

4.2. Structure analysis

Following [6], the analysis was started assuming two layers to be reconstructed as described by vertical bucklings (b) and surface parallel (p) atomic shifts in the hexagonal top layer and, by interaction, bucklings in the quadratic second layer. Subsequently, the model was extended to include four reconstructed layers. The parameters for the general model with four layers reconstructed are displayed in figure 6. They are defined to be comparable to those used in [6] and obey the mirror symmetry within the unit cell. For only two layers reconstructed, the values $p_2^i = 0$ and $b_j^{ik} = 0$ for $j = 3, 4$ are fixed.

For two layers assumed to be reconstructed and using a database with energies up to 300 eV, we obtained a satisfying fit similar to that achieved in [6] and equivalent to an average best-fit R-factor of $R_P = 0.19$. Figure 7(a) illustrates the fit quality for a selected superstructure spot. Yet, extending the maximum energy to 600 eV—and still assuming only two layers to be reconstructed—makes the average R-factor rise to $R_P = 0.26$ with, however, some superstructure beams exhibiting a much worse fit as demonstrated in figure 7(c).

Certainly, this means that some essential features of the structure are missing. As the fit quality worsens with the extension to higher energies and thus with a deeper surface penetration, this must be due to deeper layers being reconstructed. Indeed, with two more layers allowed to reconstruct according to figure 6 (with lateral shifts in the second layer included and increasing the total number of structural parameters to $N = 17$) the fit quality improves dramatically as illustrated in figure 7(d). The average R-factor for the data set up to 600 eV improves to $R_P = 0.144$ with a variance of as small as $\mathrm{var}(R_P) = 0.009$. Also, the fit for the database up to 300 eV improves to about the same level of theory–experiment comparison ($R_P = 0.138$) which is, in particular, due to the improvements achieved for fractional order beams (figure 7(b)). The structural results obtained for models with two and

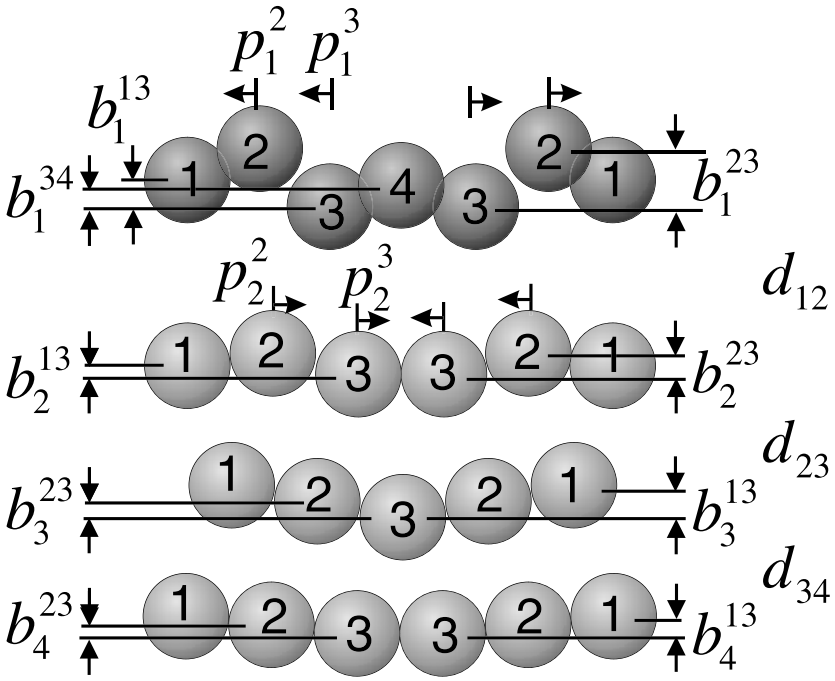

Figure 6. Model parameters to describe the full reconstruction of Ir(100)-5 × 1 with the mirror symmetry within the unit cell saved. The maximum buckling amplitudes for each layer are given on the right-hand side. Atomic numbers for the top layer correspond to figure 1 using the fact that atoms 3/5 and 2/6 are equivalent. Note that the atomic diameters, shifts and layer spacings do not scale.

four layers reconstructed and for databases 20–300 and 20–600 eV are summarized in table 2 and compared to results given in [6].

First, the reader should note that the reconstruction buckling amplitudes in the third and fourth layers are substantial. They are clearly outside the limits of errors (see section 4.3). Second, the best-fit parameters for the top two layers are—within the limits of errors—the same for the low-energy database with two layers allowed to reconstruct on the one hand and the high-energy database with four layers reconstructed on the other hand. Yet, whilst this can easily be explained by the limited depth probed at lower energies with the structure of deeper layers entering the scattering scenario with evenly limited weight, the third issue to note comes as a surprise: with always the high-energy database used, the results for the top two layers are—again within the limits of errors—independent of the number of layers allowed to reconstruct. This is in spite of the fact that the reconstructed deeper layers are involved in the total scattering. A less favourable *R*-factor (0.261 versus 0.144) only results when, contrary to reality, only two layers are allowed to reconstruct. This seems to indicate that the parameters of the first two layers are largely decoupled from those of deeper layers which demands a closer look in this respect.

4.3. Parameter correlations, sensitivity, error limits and reliability

The issue of parameter correlations, e.g. the influence of, say, the third-layer buckling on that of the second layer, is best illuminated by an *R*-factor contour plot involving these quantities. Yet,

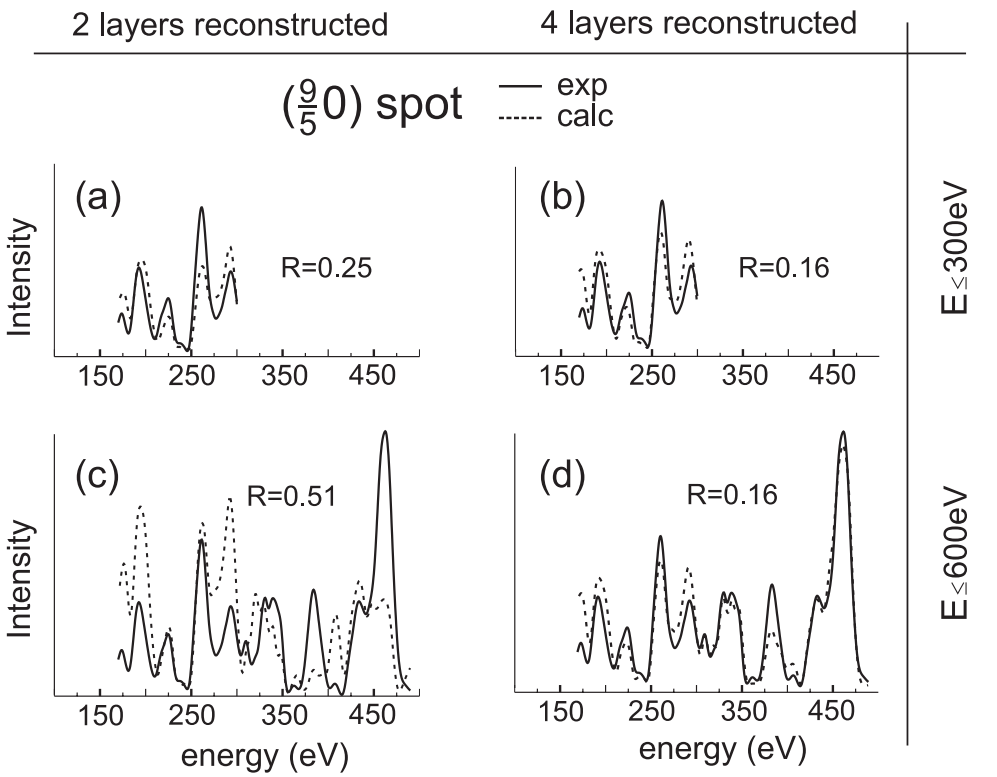

Figure 7. Comparison of the fit quality for a selected superstructure beam ($(\frac{9}{5}\ 0)$ beam) for the cases of two (a), (c) and four (b), (d) reconstructed layers of Ir(100)-5 × 1 and for a total database extending to 300 eV (a), (b) and 600 eV (c), (d) at maximum. Note that the calculated spectrum in panel (c) appears higher as it is made to fit to the average experimental intensity level. The *R*-factors given are single-beam values for the beam presented.

such a representation is complicated by two circumstances. First, the buckling of the layers is not described by a single parameter as evident from figure 6. We therefore used the maximum buckling amplitude of the layers ($b_2 = b_2^{23}, b_3 = b_3^{13}$) as parameters *and*, during their variation, made the remaining buckling parameters (b_2^{13}, b_3^{23}) scale in the same way, so that the spatial buckling characteristics of each layer was always the same. The second complication is due to the fact that a fully accurate investigation would require that at each grid point (b_2, b_3) of the two bucklings *all* other parameters must be optimized. Yet, this would cost many hundreds of CPU hours which we could not afford. So, as an approximation and as usually practised in LEED, we held all other parameters constant, in particular the spacings between the centre of mass planes of the different layers.

Figure 8 presents the respective contour map with the contour lines being approximately elliptic. As obvious, the main axes of the ellipses are almost aligned with the respective axes of the parameters b_2 and b_3, i.e., there are hardly any correlations between them. This is fully in line with the results given in table 2. Yet, we emphasize that this cannot be taken as a general feature of LEED structure determination. As an example showing the opposite we mention the case of (4 × 4)-Pb/Cu(111) which is characterized by a similarly deep-going reconstruction of the copper substrate induced by lead [23]. Rather wrong bucklings result for upper layers when those of deeper layers are not considered. Similar features were observed for the epitaxial system (4 × 4)-Pb/Co/Cu(111) with lead acting as a surfactant [24].

Table 2. Structure of Ir(100)-5 × 1 described by the parameters defined in figure 6 and resulting from different databases used (⩽600 eV, 20–600 eV; ⩽300 eV, 20–300 eV or, for comparison, 50–300 eV [6]) and a different number of layers assumed to reconstruct (2L, two layers; 4L, four layers). The parameters $\overline{d}_{ik}$ denote interlayer spacings with correspondence to the centre of mass planes of the layers, whilst d_{ik} gives the smallest spacing between their subplanes.

	This work (⩽600 eV, 4L)	This work (⩽300 eV, 4L)	This work (⩽600 eV, 2L)	This work (⩽300 eV, 2L)	Reference [6] (⩽300 eV, 2L)
R_P	0.144	0.138	0.261	0.192	0.209
d_{12} (Å)	1.94	1.94	1.94	1.94	1.944
$\overline{d}_{12}$ (Å)	2.25	2.25	2.25	2.25	
d_{23} (Å)	1.79	1.79	1.85	1.84	1.836
$\overline{d}_{23}$ (Å)	1.88	1.88	1.88	1.88	
d_{34} (Å)	1.83	1.83			
$\overline{d}_{34}$ (Å)	1.93	1.94			
d_{45} (Å)	1.89	1.90			
$\overline{d}_{45}$ (Å)	1.91	1.92			
b_1^{13} (Å)	0.25	0.25	0.26	0.25	0.257
b_1^{23} (Å)	0.55	0.55	0.55	0.53	0.527
b_1^{34} (Å)	0.20	0.20	0.21	0.20	0.20
p_1^2 (Å)	0.05	0.05	0.05	0.05	0.03
p_1^3 (Å)	0.07	0.07	0.07	0.07	0.078
b_2^{13} (Å)	0.07	0.08	0.06	0.07	0.073
b_2^{23} (Å)	0.10	0.10	0.09	0.10	0.098
p_2^2 (Å)	0.01	0.02			
p_2^3 (Å)	0.02	0.03			
b_3^{13} (Å)	0.10	0.11			
b_3^{23} (Å)	0.05	0.06			
b_4^{13} (Å)	0.06	0.06			
b_4^{23} (Å)	0.03	0.03			

To demonstrate the sensitivity of our fit with respect to the parameters, figure 9 presents a cut through the above R-factor map as function of b_2 as an example, with b_3 and (again) all other parameters fixed at their best-fit values. For comparison the same fit is shown also for the 300 eV data set. As obvious, the broader and higher-energy database produces a lower R-factor variance and a steeper R-factor curve. Similar to the case of the 1 × 1 phase, both effects add to reduce the error limits which can be read from the intersections of the respective variance levels with the corresponding R-factor curves.

Though the buckling parameters between the top two and deeper layers appear to be largely decoupled, there can be correlations between the remaining parameters. Therefore, in order to estimate the error for a single parameter, e.g., b_2^{23} or b_3^{13}, *and* to simultaneously get rid of any parameter correlations for the retrieval of realistic error limits, we undertook the effort to optimize all other parameters. This is except for lateral displacements which were fixed at $p_j^i = 0$, so that the resulting minimum R-factor is slightly increased over the absolute minimum. The corresponding R-factor plots are given in figure 10 whereby Δb denotes the deviation from the best-fit value for b_2^{23} and b_3^{13}. From the variance level of the R-factor the statistical errors for b_2^{23} and b_3^{13} result as 1.8×10^{-2} and 2.4×10^{-2} Å, respectively. As expected, the error for the deeper layer is larger due to electron attenuation. Comparison to the variance level intersections in figure 9 (high-energy data set) shows that the error limit

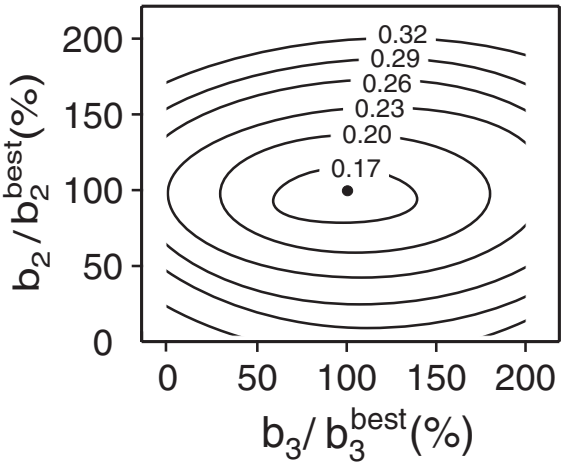

Figure 8. *R*-factor contour plot for the maximum buckling amplitudes in the second and third layers whereby the spatial buckling characteristics of the layers were held constant. Also, all other parameters were fixed at their best-fit values. The buckling amplitudes are relative to the respective best-fit values given in table 2.

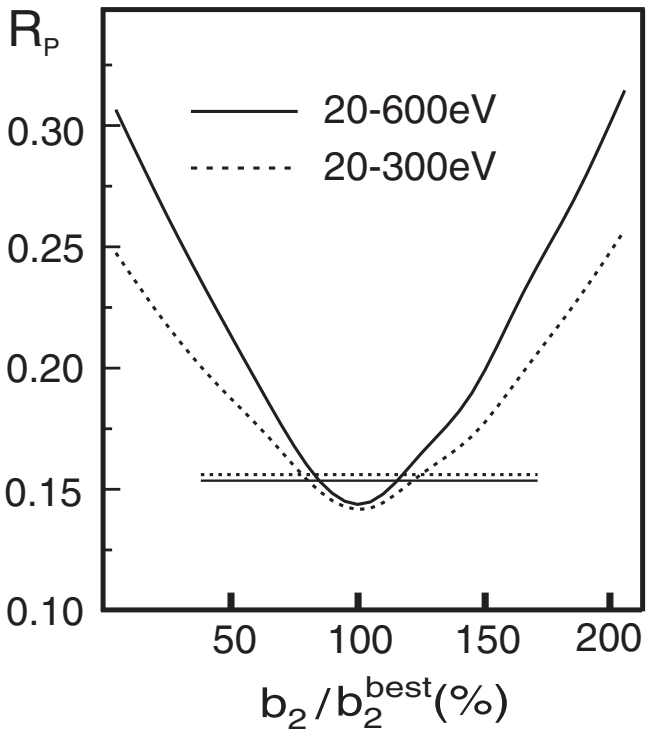

Figure 9. *R*-factor dependence on the maximum second-layer buckling amplitude b_3 (with the spatial buckling characteristics of the layer fixed) for different energy ranges applied in the analysis.

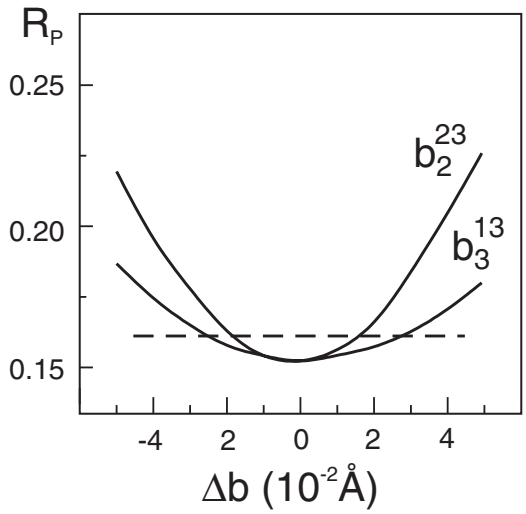

Figure 10. *R*-factor dependence for the 600 eV data set on the single-layer buckling amplitudes b_2^{23} and b_3^{13} (see model in figure 6) with all other parameters optimized in each case.

for b_2 ($\hat{=}b_2^{23}$) is only slightly higher when parameter correlations are unconsidered. If we take—to be on the safe side—a factor of two into consideration, the statistical errors for the remaining parameters can be estimated to amount to ±0.01–0.02 Å for interlayer spacings and the buckling amplitudes in the first and second layer, and ±0.02–0.03 Å for the bucklings in deeper layers and the lateral shifts in the top two layers.

Finally, we address the issue of reliability of our structure determination. As described, a total of $N = 17$ geometrical parameters were determined. Assuming that each peak in an $I(E)$ spectrum (peak width $4V_{0i}$) carries independent structural information leads to a minimum requirement for the database width, $\Delta E_{min} = 4NV_{0i}$. With $V_{0i} = 5$ eV, a value of $\Delta E_{min} = 340$ eV results. Given our total database, $\Delta E = 10\,508$ eV, a redundance factor of as much as $\Delta E/\Delta E_{min} \approx 30$ results. Besides the convincingly low *R*-factor achieved, this puts our analysis on very safe statistical grounds. Also, the reader should note the excellent agreement of our results with those of Johnson *et al* [6] for the subset of parameters investigated in both analyses. As evident from table 2, discrepancies between parameters are never larger than 0.02 Å, in most cases smaller or even vanishing within the digits given. This is the more remarkable as the two investigations are completely independent from each other, with different sample preparations, different intensity measurement procedures, different intensity calculation codes and different structural search strategies involved. If the two analyses do not happen to suffer from some (same) systematic errors (not included in the above statistical error estimation), the resulting situation concerning the standards of quantitative LEED seems to be more favourable than a number of years ago. Then, in a concerted action, different laboratories analysed the (much simpler) surface of Cu(100) resulting in considerable deviations from each other [25, 26].

5. Conclusion

We have shown that the reconstruction of Ir(100)-5 × 1 extends considerably deeper into the surface than anticipated before. The second and third layers are substantially buckled (total amplitude 0.10 Å) and even the fourth layer is still modified (total buckling 0.06 Å).

The detection of this deep-going reconstruction by quantitative LEED comes only by the use of sufficiently high electron energies which allow us to probe deeper layers with sufficient sensitivity. Simultaneously, the higher energies applied lead to an increased database for the structure determination. As a result, the R-factor dependence on a certain parameter becomes steeper and the variance of the R-factor gets smaller. Both effects add to reduce the limits of statistical errors as demonstrated for both the 1×1 and 5×1 phases of Ir(100). In the investigation presented for the 5×1 phase a database width of more than 10.000 eV entered the analysis putting the determination of as much as 17 geometrical parameters on safe statistical grounds. Together with a minimum Pendry R-factor of $R_P = 0.144$, which is convincingly low in view of the complexity of the structure, error limits in the picometre range are estimated.

Surprisingly, the structural parameters for the top two layers, retrieved with assuming only these layers to be reconstructed, are—within the limits of errors—the same as when the full four-layer reconstruction is considered. Obviously, couplings between single parameters are to a large extent averaged out by effective multi-parameter correlations: a wrong choice for a small subset of parameters leads to only negligible errors in all other parameters. Though this cannot be taken as a general feature of quantitative LEED, it allows us to compare our results to those obtained independently earlier assuming, however, only two layers to be reconstructed [6]. Within the (small) limits of errors the same parameter values result. This demonstrates the reliability of today's quantitative LEED.

Acknowledgment

This work was supported by Deutsche Forschungsgemeinschaft (DFG).

References

[1] Ignatiev A, Jones A V and Rhodin T N 1972 *Surf. Sci.* **30** 573
[2] Van Hove M A, Koestner R J, Bibérian P C, Kesmodel L L, Bartoš I and Somorjai G A 1981 *Surf. Sci.* **103** 189
[3] Lang E, Müller K, Heinz K, Van Hove M A, Koestner R J and Somorjai G A 1983 *Surf. Sci.* **127** 347
[4] Moritz W, Müller F, Wolf D and Jogodzinski H 1983 *Book 9th Vacuum Congr. 5th Int. Conf. on Solid Surfaces (Madrid)* p 70 (Abstracts)
[5] Bickel N and Heinz K 1985 *Surf. Sci.* **163** 435
[6] Johnson K, Ge Q, Titmuss S and King D A 2000 *J. Chem. Phys.* **112** 10460
[7] Ge Q, King D A, Marzari N and Payne M C 1998 *Surf. Sci.* **418** 529
[8] Gilarowsky G, Méndez J and Niehus H 2000 *Surf. Sci.* **448** 290
[9] Rhodin T N and Brodén G 1976 *Surf. Sci.* **60** 466
[10] Küppers J and Michel H 1979 *Appl. Surf. Sci.* **3** 179
[11] Heinz K, Schmidt G, Hammer L and Müller K 1985 *Phys. Rev.* B **32** 6214
[12] Rous P J, Pendry J B, Saldin D K, Heinz K, Müller K and Bickel N 1986 *Phys. Rev. Lett.* **57** 2951
[13] Rous P J 1992 *Prog. Surf. Sci.* **39** 3
[14] Heinz K 1995 *Rep. Prog. Phys.* **58** 637
[15] Blum V and Heinz K 2001 *Comput. Phys. Commun.* **134** 392
[16] Rundgren J 1999 private communication
[17] Kottcke M and Heinz K 1997 *Surf. Sci.* **376** 352
[18] Pendry J B 1980 *J. Phys. C: Solid State Phys.* **13** 937
[19] Hebenstreit W, Ritz G, Schmid M, Biedermann A and Varga P 1997 *Surf. Sci.* **388** 150
[20] Heilmann P, Heinz K and Müller K 1979 *Surf. Sci.* **83** 487
[21] Heinz K, Lang E, Strauss K and Müller K 1982 *Surf. Sci.* **120** L401
[22] Giesen M 2001 *Prog. Surf. Sci.* **68** 1
[23] Müller S, Prieto J E, Rath C, Hammer L, Miranda R and Heinz K 2001 *J. Phys.: Condens. Matter* **13** 1793
[24] Müller S, Prieto J E, Krämer Th, Rath C, Hammer L, Miranda R and Heinz K 2001 *J. Phys.: Condens. Matter* **13** 10647
[25] Jona F 1987 *Surf. Sci.* **192** 398
[26] Jona F, Jiang P and Marcus P M 1987 *Surf. Sci.* **192** 414